Broadband low-frequency sound isolation by lightweight adaptive metamaterials

Yunhong Liao,[1] Yangyang Chen,[2] Guoliang Huang,[2] and Xiaoming Zhou[1,3,a)]
[1]*Key Laboratory of Dynamics and Control of Flight Vehicle, Ministry of Education and School of Aerospace Engineering, Beijing Institute of Technology, Beijing 100081, People's Republic of China*
[2]*Department of Mechanical and Aerospace Engineering, University of Missouri, Columbia, Missouri 65211, USA*
[3]*State Key Laboratory of Explosion Science and Technology, Beijing Institute of Technology, Beijing 100081, People's Republic of China*

(Received 31 October 2017; accepted 25 November 2017; published online 20 December 2017)

Blocking broadband low-frequency airborne noises is highly desirable in lots of engineering applications, while it is extremely difficult to be realized with lightweight materials and/or structures. Recently, a new class of lightweight adaptive metamaterials with hybrid shunting circuits has been proposed, demonstrating super broadband structure-borne bandgaps. In this study, we aim at examining their potentials in broadband sound isolation by establishing an analytical model that rigorously combines the piezoelectric dynamic couplings between adaptive metamaterials and acoustics. Sound transmission loss of the adaptive metamaterial is investigated with respect to both the frequency and angular spectrum to demonstrate their sound-insulation effects. We find that efficient sound isolation can indeed be pursued in the broadband bi-spectrum for not only the case of the small resonator's periodicity where only one mode relevant to the mass-spring resonance exists, but also for the large-periodicity scenario, so that the total weight can be even lighter, in which the multiple plate-resonator coupling modes appear. In the latter case, the negative spring stiffness provided by the piezoelectric stack has been utilized to suppress the resonance-induced high acoustic transmission. Such kinds of adaptive metamaterials could open a new approach for broadband noise isolation with extremely lightweight structures. *Published by AIP Publishing.* https://doi.org/10.1063/1.5011251

I. INTRODUCTION

Airborne noise emerges in many circumstances, from industrial production, transportation, urban construction, to aeronautics and astronautics, and has been found to be harmful to human's physical and mental health. Broadband noise isolation is in demand and is being made possible using various kinds of materials and structures;[1–4] however, the challenge has not been tackled yet. Especially for low-frequency noises, conventional sound insulation materials or structures are usually bulky and heavy, therefore they are hardly implemented in a practical environment. For instance, foam materials with micro-scale porous microstructures, which have been widely used in industries nowadays, absorb sounds by increasing the air resistance; acoustic energy is finally dissipated as heat. However, they cannot attenuate low-frequency sounds very well because of the weak viscous friction of the air oscillation.[1] Micro-perforated plates with small holes punched in a thin flat plate offer an alternative porous absorber and suffer likewise from the weak absorption of low-frequency sounds. New mechanisms are in demand to overcome this challenging issue.

Experiencing rapid development in the past decade, acoustic metamaterials have opened a new route to the low-frequency noise suppression with compact and lightweight structures. Acoustic metamaterials are artificial composite materials with carefully designed microstructures. They utilize the local resonance to create anomalous dynamic properties, including negative dynamic mass[5–7] or negative modulus;[8] at corresponding frequencies, they are opaque for sound waves, providing novel technological concepts for noise reduction. For low-frequency sound insulation, membrane-type acoustic metamaterials have been proposed.[9,10] They are made of stretched membranes fixed on a rigid frame and additional mass blocks are attached to the membrane's surface. A very high sound transmission loss (STL) can be acquired near the anti-resonant frequency of the membrane structure, which is determined by the weight of the mass and the pre-tension of the membrane.[11–13] Further studies investigated membrane-type metamaterials with different resonant frequencies in order to achieve broadband sound attenuations.[14,15] The plate-type metamaterials, which are of the nontrivial bending rigidity, are also proposed for sound reductions. Compared with the membrane-type one, the plate-type metamaterial has superior performances not only in the frequency response but also in the angular spectrum of sound transmission.[16–19] However, the local resonance utilized in either membrane-type or plate-type acoustic metamaterials inevitably leads to narrow frequency band of noise isolations.

To broaden the operation bands, researchers introduced active metamaterials with tunable resonant frequencies. For instances, a thin-film structure attached to an enclosed cavity filled with the high-pressure air was designed. The eigenfrequency of the thin film can be tuned by applying different air pressures.[20] Active nonlinear metamaterials with the varactor diode have also been reported to regulate the sound

a)Author to whom correspondence should be addressed: zhxming@bit.edu.cn

transmission by adjusting the input power.[21] In addition, the external magnetic field has been employed to change the pretension of a magnetorheological elastomer membrane,[22] and the resonant frequency could be modulated. Researchers utilized the amplitude and phase of the voltage induced by external electrical circuits to tune the acoustic performance of membranes.[23] By placing a loudspeaker inside the resonators, the sound insulation performance could be actively tailored through a feedforward control strategy.[24] Piezoelectric materials attracted lots of interests due to their small size, light weight, and easy tunability. They have been implemented in several plate structures, making the STL peak frequencies tunable by the means of the shunted inductance circuit.[25,26] Up till date, researchers have proposed various types of active acoustic metamaterials with tunable properties. However, most of the designs, though being tunable, operated still for narrow-band excitations. They are not responsible sufficiently well to the full-frequency-spectrum noise excitations. Achieving broadband sound insulations with lightweight structures still remains a challenging issue and has never been entirely resolved even with the metamaterial concept.

Recently, Chen *et al*. proposed a new class of adaptive metamaterials in which the structure-borne bandgap has been extremely broadened. In their design, both negative capacitance and inductance are incorporated into the shunting circuit.[27] Due to the existence of the coincidence effect between the structure vibration and acoustics, it is expected that their adaptive metamaterials could be potentially applicable to the broadband sound reduction. In this work, we intend to verify the phenomena by developing an analytical model considering structure–acoustic interactions. The paper is arranged as follows: In Sec. II, we first recall the adaptive metamaterial with the negative capacitance and negative inductance in the shunting circuit and then establish an analytical model considering their interactions with acoustic waves impinged from arbitrary incident angles. In Sec. III, numerical results regarding cases of both small and large periodicities of adaptive resonators will be analyzed, clearly verifying its broadband sound-isolation behavior. A brief summary is outlined in Sec. IV.

II. ANALYTIC MODEL OF ACTIVE ACOUSTIC METAMATERIALS

Figure 1 shows the schematic of the adaptive acoustic metamaterial, which is composed of a thin plate attached periodically with mass-spring resonators, and is illuminated by a plane acoustic wave of arbitrary incident angles. The weight of the attached mass is m_1, and the periodicity between adjacent resonators is L. The background medium is the air with mass density ρ_0 and sound velocity c_0. In the usual case that the stiffness coefficient k_1 is the positive constant, the described model has been investigated previously in the framework of dynamic homogenization.[18] In contrast, the present study focuses on the case that the stiffness coefficient k_1 is frequency-dependent, which can be practically realized by the hybrid circuit shunted piezoelectric stack.[27] This would allow us to modulate the shunting circuits in order to achieve the high transmission loss in the broad

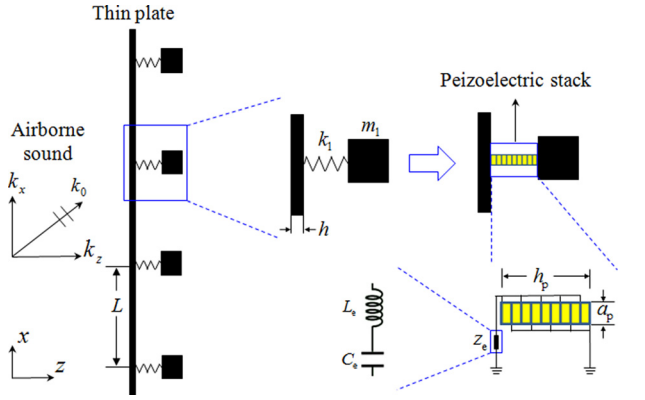

FIG. 1. Schematic of acoustic model developed for evaluating the sound-insulation effect of the adaptive metamaterials. The metamaterial consists of the thin plate on which the mass block and the hybrid shunted piezoelectric stacks are attached and it is impinged by a plane acoustic wave of arbitrary incident angle.

frequency band, which is unavailable by the composite plate with passive resonators.

Let us first recall the overall mechanical property of the piezoelectric stack, in order to clearly identify their effects on broadband sound insulation. The piezoelectric stack is made of the N-layers of piezoelectric plates, and the adjacent plate is polarized in opposite directions and individually shunted with the hybrid circuits involving the negative capacitance C_e and negative inductance L_e. Consider the vibration along the z direction only. The constitutive equation of the piezoelectric plate reads[27]

$$S_z = d_{33}E_z + s_{33}T_z, \tag{1}$$

$$D_z = \varepsilon_{33}E_z + d_{33}T_z, \tag{2}$$

where S_z and T_z are strain and stress, D_z and E_z are the electric displacement and electric field. The constitutive parameters d_{33}, s_{33}, and ε_{33} are the piezoelectric coefficient, elastic compliance, and dielectric constant, respectively. The piezoelectric material used in this study is of the type PMN-33%PT with material parameters $d_{33} = 2820.0 \times 10^{-12}\mathrm{C/N}$, $s_{33} = 119.6 \times 10^{-12}\mathrm{m^2/N}$, and $\varepsilon_{33} = 8200\varepsilon_0$, where ε_0 is the vacuum dielectric constant. By incorporating the electric impedance Z_e that arises from the shunting circuit, one can write the effective modulus of the piezoelectric stack as[28]

$$E_p = \frac{E_0}{1 - \dfrac{k_{33}^2}{1 + 1/(i\omega C_p Z_e)}}, \tag{3}$$

where $k_{33} = d_{33}/\sqrt{\varepsilon_{33}s_{33}}$ is the electromechanical coupling coefficient, $E_0 = 1/s_{33}$ is the short-circuit modulus, $C_p = \frac{N^2 a_p^2 \varepsilon_{33}}{h_p}$ is the capacitance of the piezoelectric stack, where $h_p = 10a_p = 10\,\mathrm{mm}$ is taken. The impedance is $Z_e = \frac{1}{i\omega C_e} + i\omega L_e$ for the circuit in which the capacitance and inductance are connected in series. In terms of the circuit parameters, we can rewrite Eq. (3) as

$$\frac{E_p}{E_0} = 1 + \frac{k_{33}^2}{\left(1 - k_{33}^2\right) + \left(C_e/C_p\right)/\left(1 - \omega^2/\omega_e^2\right)}, \tag{4}$$

where $\omega_e = 1/\sqrt{L_e C_e}$ is the resonant frequency of the shunting circuit. Reasonably considered as a spring, the piezoelectric stack takes the stiffness coefficient $k_1(\omega) = E_p a_p^2/h_p$.[27] Figure 2(a) shows the normalized effective modulus E_p/E_0 against the normalized frequency ω/ω_e for the specific value $C_e/C_p = -0.8$. It is worth to emphasize that the directly proportional relationship between the two parameters, available only if $L_e, C_e < 0$, is critical to the realization of broadband sound isolation, as will be explained later. Furthermore, effective modulus at zero frequency can vary drastically for different circuit capacitances, as depicted in Fig. 2(b), being even negative in the range $-1 < C_e/C_p < k_{33}^2 - 1$. This would result in the negative $k_1(\omega)$ band below a cut-off, showing later the great value upon the removing of low-frequency resonant transmission in the large-periodicity case.

Let a plane acoustic wave incident on the thin plate with active springs. The coupled acoustic-structure interaction is to be analyzed for a full evaluation of the sound blockage effect of the adaptive metamaterial. The equation of motion of the composite plate subject to acoustic loads is written with the transverse displacement w by[18]

$$D_p \frac{\partial^4 w}{\partial x^4} + \rho h \frac{\partial^2 w}{\partial t^2} - \sum_{n=-\infty}^{+\infty} F\delta(x - nL) - \rho_0 \left(\frac{\partial \psi_I}{\partial t} - \frac{\partial \psi_T}{\partial t} \right) = 0, \tag{5}$$

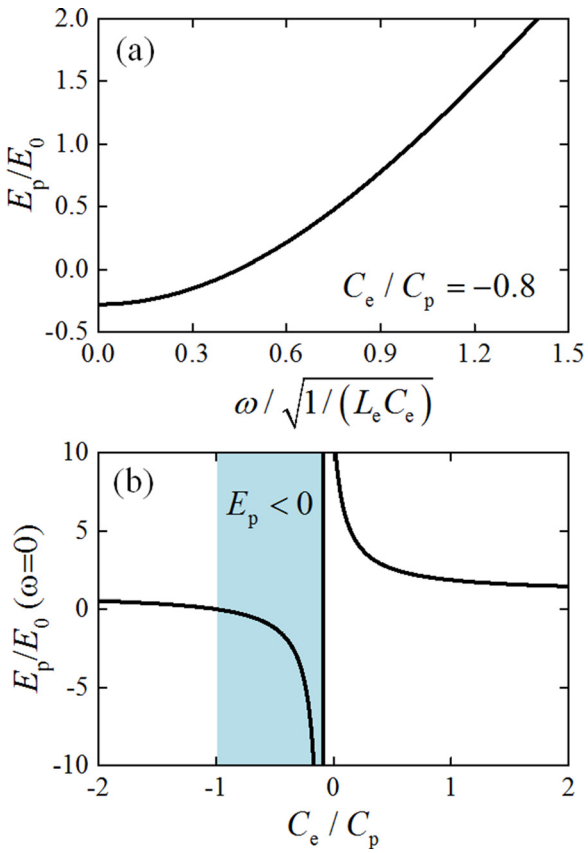

FIG. 2. (a) The normalized effective modulus E_p/E_0 of the piezoelectric stack computed at various frequencies according to Eq. (4) with the parameter $C_e/C_p = -0.8$. (b) Effective modulus at zero frequency against different circuit capacitances C_e/C_p.

where the bending stiffness of the thin plate is $D_p = E_Y h^3/[12(1-\nu^2)]$ with the Young's modulus E_Y and Poisson's ratio is ν. The density of the plate is ρ, and the thickness is h. Note that the formulation (5) is unchanged in form, regardless of passive and active springs included in the model. The force adhered to the active spring $k_1(\omega)$, which is dependent on frequency, can be derived as

$$F = \frac{m_1 \omega^2 k_1(\omega)}{k_1(\omega) - m_1 \omega^2} w(nL, t). \tag{6}$$

This equation can also be obtained by simply replacing the spring coefficient with $k_1(\omega)$ in the passive structure.[18] It is due to this reason that one would find the analogous equation systems to the passive ones. Nevertheless, for the completeness of the study, formulations critical to the understanding of the issue and those pertaining to the active springs $k_1(\omega)$ will be described below, while other details may be found in the passive scenario.[18]

Owing to the periodic arrangement of resonators, the plate displacement can be expressed as the superposition of harmonics of different orders, written by

$$w(x,t) = \sum_{n=-\infty}^{+\infty} A_n e^{-i\left(k_x + \frac{2n\pi}{L}\right)x} e^{i\omega t}, \tag{7}$$

where A_n is the complex amplitude of the nth-order flexural mode of the plate. Likewise, the velocity potentials of acoustic fields, ψ_I and ψ_T, in the incident and transmitted regions, respectively, are expressed as

$$\psi_I = e^{-i(k_z z + k_x x)} e^{i\omega t} + \sum_{n=-\infty}^{+\infty} B_n^- e^{-i\left[-k_{zn} z + \left(k_x + \frac{2n\pi}{L}\right)x\right]} e^{i\omega t}, \tag{8}$$

$$\psi_T = \sum_{n=-\infty}^{+\infty} B_n^+ e^{-i\left[k_{zn} z + \left(k_x + \frac{2n\pi}{L}\right)x\right]} e^{i\omega t}, \tag{9}$$

where B_n^+ and B_n^- are unknown complex amplitudes of wave transmission and reflection and the unity intensity of incident wave has been assumed. The z-component of acoustic wavevector k_{zn} is defined as

$$k_{zn} = \begin{cases} \sqrt{k_0^2 - (k_x + 2n\pi/L)^2}, & k_0 \geq k_x + 2n\pi/L \\ -i\sqrt{(k_x + 2n\pi/L)^2 - k_0^2}, & k_0 \leq k_x + 2n\pi/L, \end{cases} \tag{10}$$

where $k_0 = \omega/c_0$ is the wave number in air. Consider the continuity condition of velocities at the interfaces between the plate and acoustic region, as well as the virtual work principle. The complex coefficients A_n can be finally computed from the following equation that has involved the acoustic–structure interaction:

$$\left[D_p \left(k_x + \frac{2n\pi}{L} \right)^4 - \rho h \omega^2 + \frac{2i\omega^2 \rho_0}{k_{zn}} \right] A_n - \frac{1}{L} \frac{m_1 \omega^2 k_1(\omega)}{k_1(\omega) - m_1 \omega^2} \times \sum_{q=-\infty}^{+\infty} A_q = \begin{cases} 2i\omega\rho_0, & n = 0 \\ 0, & n \neq 0. \end{cases} \tag{11}$$

The complex amplitudes of acoustic waves can be obtained by

$$B_n^- = \begin{cases} 1 - \dfrac{\omega A_n}{k_{zn}}, & n = 0 \\ -\dfrac{\omega A_n}{k_{zn}}, & n \neq 0, \end{cases} \tag{12}$$

$$B_n^+ = \frac{\omega A_n}{k_{zn}}. \tag{13}$$

The energy transmission and reflection coefficients of acoustic waves are computed, respectively, by

$$T_{\mathrm{ac}} = \sum_{n=-\infty}^{+\infty} |B_n^+|^2 \mathrm{Re}(k_{zn})/k_{z0}, \tag{14}$$

$$R_{\mathrm{ac}} = \sum_{n=-\infty}^{+\infty} |B_n^-|^2 \mathrm{Re}(k_{zn})/k_{z0}. \tag{15}$$

III. RESULTS AND DISCUSSION

As an example, an epoxy plate with material parameters $E_{\mathrm{Y}} = 3.9\,\mathrm{GPa}$, $v = 0.4$, $\rho = 1400\,\mathrm{kg/m^3}$, and the thickness $h = 0.4\,\mathrm{mm}$ is considered. The mass density and sound velocity of the air are taken as $\rho_0 = 1.25\,\mathrm{kg/m^3}$ and $c_0 = 343\,\mathrm{m/s}$. Figure 3 shows the eigen-frequencies at different periodicity L of the composite unit with and without passive resonators of parameters $k_1 = 0.1\,\mathrm{kN/mm}$ and $m_1 = 5\,\mathrm{g}$ (with the resonant frequency 712 Hz). The eigen-frequency curve of the composite plate is found to follow that of either the single plate of the width L or single resonator in the length scales of L far away from their crossover region, while the hybridization happens near the cross, as discovered previously.[18] These frequencies measure exactly the anti-resonance frequencies of acoustics, at which sound transmission loss approaches the maximum.

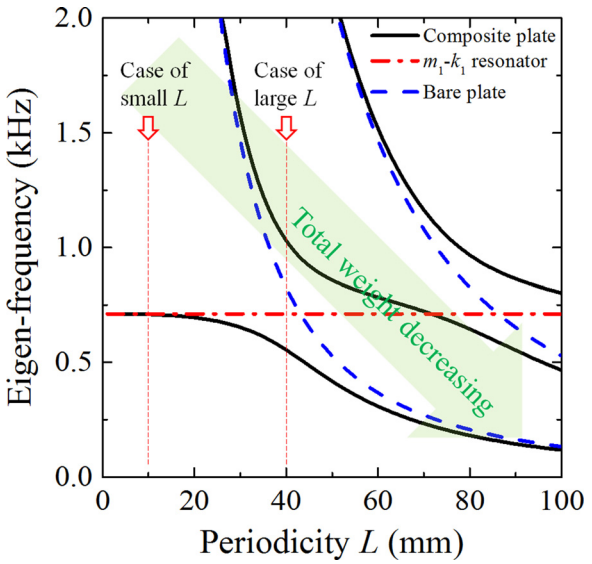

FIG. 3. The eigen-frequencies at different periodicity L for the composite unit involving passive resonators of the resonant frequency 712 Hz (solid line), and the results of the single plate of the width L (dashed line) and single resonator (dashed-dotted line) are also provided for comparison.

Unfortunately, the anti-resonance points are always accompanied by the resonant acoustic transmission. In previous studies, the resonant induced complete transmission has been used to prevent the decaying of evanescent waves in the hyperlens[29] or realize the frequency-controlled acoustic directive radiation;[18] yet, it must be avoided here regarding the broadband sound blockage. In the frequency range of interest, it is seen that in the case of relatively small periodicity L, the composite plate shows only one branch of high STL modes that is governed by the resonator's resonance. In order for the lighter weight of composite structures, the large periodicity L needs to be considered, in which case, more branches of high STL modes will appear, meaning that there would exist more resonant transmission peaks. This imposes a challenging problem of how to maintain high transmission loss over broadband frequencies, and eliminate unwanted resonant transmissions in the mean time. In the following, the scenarios of the small ($L = 10\,\mathrm{mm}$) and large ($L = 40\,\mathrm{mm}$) periodicities are examined separately from which different strategies will be proposed.

A. Small periodicity ($L = 10\,\mathrm{mm}$) case

Figure 4(a) shows the normal-incidence STL spectrum for the case with small periodicity $L = 10\,\mathrm{mm}$. It is seen that the added resonator has produced an STL peak at its resonant frequency 712 Hz, which is accompanied by a resonant transmission at a higher frequency (977 Hz). Due to the coincidence effect, these two frequencies can be predicted by the band structure of flexural wave modes of the composite plate and they correspond to frequencies at the Brillouin zone boundary and zero point, respectively, as shown in Fig. 4(b). Figure 4(c) gives the contour plot of the STL against both the frequency and angular spectra. Provided that the sound isolation beyond the threshold 20 dB is useful, it is clear that the high STL due to the resonator is available only in the very narrow frequency band. One route to enlarge the bandwidth is to increase the weight of attached mass, as verified in Fig. 5(a), wherein the spring coefficient is increased proportionally such that the resonant frequency 712 Hz remains constant. The composite structure must be heavy if designed in this way. Here, we intend to enhance the frequency bandwidth without adding additional weights. Now, let us plot the STL spectrum at different stiffness coefficients of the spring, while keeping the small weight 5 g of the attached mass unchanged. It is found that the sound-insulation bandwidth can be increased accompanied by the increasing critical frequency pertaining to the STL peak. We see that the spring coefficient has to be dependent on the frequency in order to trace the high STL trajectory. There is an important finding made by Chen *et al.*[27] that the required frequency dispersion of the spring coefficient is in good agreement with that exhibited by piezoelectric stacks with the shunting circuit of $L_{\mathrm{e}}, C_{\mathrm{e}} < 0$. Then, we optimize circuit parameters and get $C_{\mathrm{e}} = -C_{\mathrm{p}}$, $L_{\mathrm{e}} = -15.39\mathrm{H}$, $N = 7$, so that the spring dispersion has been made very close to the peak STL curve, as shown by the dashed line in Fig. 5(b). Figures 4(d), 4(e), and 4(f) show, respectively, the normal-incidence STL spectrum, band structure, and bi-spectrum STL contour for the composite plate with the designed active spring. In contrast

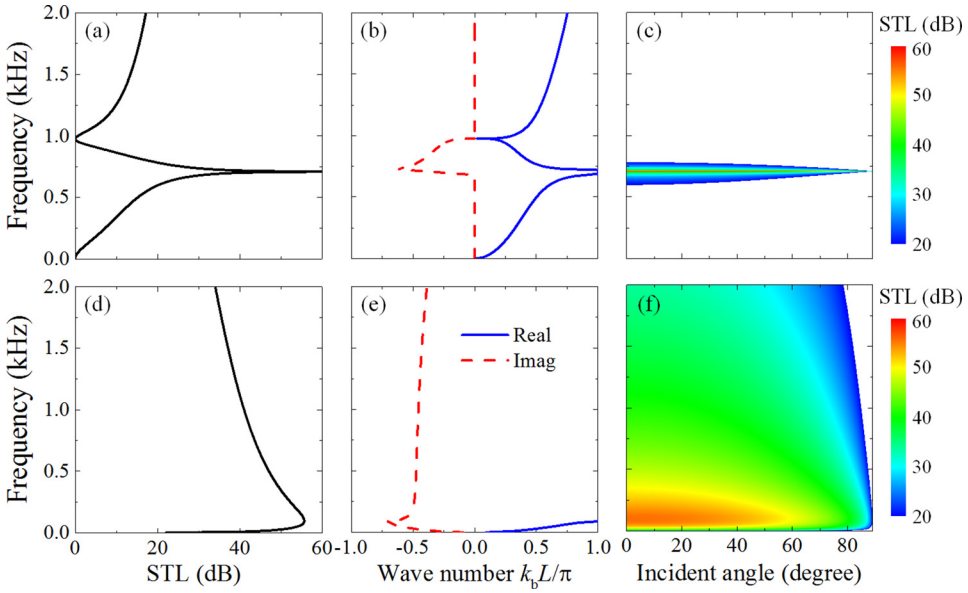

FIG. 4. (a) The normal-incidence STL spectrum, (b) complex band structure, and (c) bi-spectrum STL contour for the metamaterial of the periodicity $L = 10$ mm without involving active elements; (d), (e), and (f) are the corresponding results for the adaptive metamaterial with hybrid shunting circuits.

to the passive structure, the active composite plate has attained over 30 dB STL in the broad band ranging from 10 to 2000 Hz and for the very wide range of angles of incidence. These superior sound-insulation behaviors may be also inferred from the complex band structure. It is seen that the imaginary part of wave numbers of flexural vibration, which measures the wave dissipation, has been enhanced in magnitude in the wide frequency range. As a summary for this case, we have chosen a small weight of the attached mass, and still achieved the efficient sound isolation by introducing the active springs, whose weight can be very small practically. The results clearly identify the sound blockage effect of the lightweight adaptive metamaterials. In the next example, the case of large periodicity $L = 40$ mm will be examined in order for the further decrease of the composite mass density.

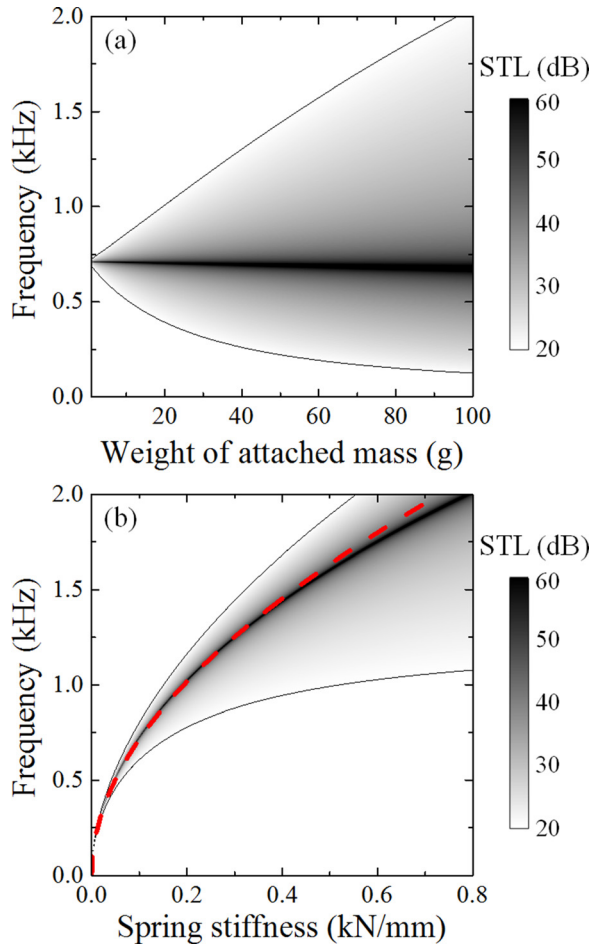

FIG. 5. (a) The STL spectrum plotted for different weights of attached mass block, where the spring coefficient is increased proportionally so that the resonant frequency 712 Hz remains constant; (b) the STL results at different stiffness coefficients of the connecting spring, in which the dashed line refers to the spring dispersion that has been designed very close to the peak STL trajectory.

B. Large periodicity ($L = 40$ mm) case

Figure 6 shows the results for the composite plate with $L = 40$ mm in a similar fashion to Fig. 4. Different from the small-periodicity case, there appears more resonant modes for the large L due to the flexural vibration of the plate. Two anti-resonance frequencies, 555 Hz and 1030 Hz, emerge as shown in Fig. 3. Correspondingly, as shown in Fig. 6(a), complete acoustic transmission occurs at two resonant frequencies, 596 Hz and 1060 Hz. According to the contour plot of the STL in Fig. 6(c), these resonant transmissions happen also in the broad angle of oblique incidence. They need to be eliminated regarding the broadband sound isolation. Following the same concept as developed in the small-L case, we examine the STL response for different spring coefficients, as given in Fig. 7. The phenomenon becomes rather complex compared with that in the small-L case. It is found that the STL peak trajectory starts from a finite cut-off frequency, below which the low sound insulation is induced by the plate vibration mode, whose frequency response is almost irrelevant to the change of spring stiffness. The strategy we proposed here is to let the active spring's dispersion match the trajectory, while negative spring stiffness is set below the cut-off in order to eliminate the acoustic resonance. The circuit parameters are optimized to be $C_e = -0.89C_p$, $L_e = -22$H, and $N = 6$. Figures 6(d) and 6(f) show the normal-incidence and bi-spectrum STL

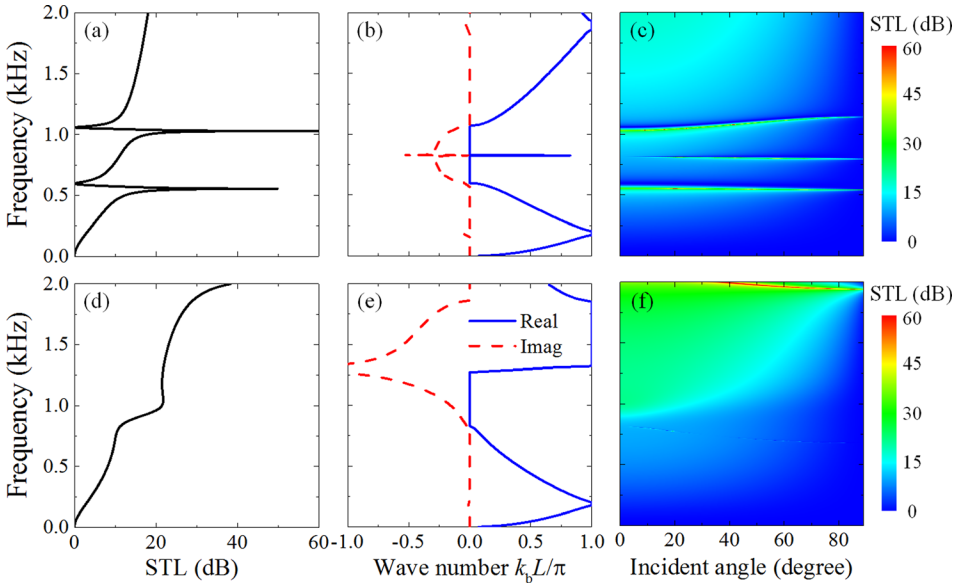

FIG. 6. (a) The normal-incidence STL spectrum, (b) complex band structure, and (c) bi-spectrum STL contour for the metamaterial of the periodicity $L = 40$ mm without involving active elements; (d), (e), and (f) are corresponding results for the adaptive metamaterial with hybrid shunting circuits.

of the composite plate equipped with this active spring. Compared with the results of the passive structure, it is seen that the STL in the active case has been enhanced in the broad frequency and angular bands. It is equally important that resonant transmissions have been eliminated from the whole spectrum of interest.

According to the analyses conducted in cases of both the small and large periodicities, active springs with the dispersive stiffness have been demonstrated to be vital to the broadband sound isolation without resonant transmissions. The negative capacitance and negative inductance, which can be truly realized by electronic techniques, are necessarily required in the shunting circuit. The studied lightweight active structure is expected to open a new avenue towards the full-spectrum noise isolation.

IV. CONCLUSION

In the preceding study, the authors have proposed a new class of adaptive metamaterials that could attain super broadband structure-borne bandgaps. Driven by the strong motivation for the noise control applications, this study intends to evaluate their potentials of broadband sound insulation. To this end, an analytical acoustic model has been developed, properly taking into account the dynamic couplings among the host plate, attached resonators, and active springs. The scenarios of the small ($L = 10$ mm) and large ($L = 40$ mm) periodicities are exemplified separately from which different strategies have been proposed. In the general sense, the dispersive feature of the spring stiffness realized by the piezoelectric stack plays a vital role in broadening the sound-isolation band. In the small-periodicity case, there exists only one branch of high STL modes governed by the resonator. Results show that over 30 dB STL has been achieved by the adaptive metamaterials in the broad band ranging from 10 to 2000 Hz and for the very wide range of angles of incidence. The acoustic phenomenon becomes rather complex in the case of large periodicity, where there exist more resonant transmissions. The challenge arises on how to maintain high STL over the broad frequency band and eliminate unwanted resonant transmissions simultaneously. The proposed strategy is to enable the spring's dispersion to match the high STL trajectory, while a negative spring stiffness is used to eliminate acoustic resonance. Numerical results clearly verify the enhanced STL and broadband sound blockage without resonant transmissions. Adaptive metamaterials of this kind are lightweight and practically realizable. They are expected to pave a new route towards the broadband control of noises and vibrations.

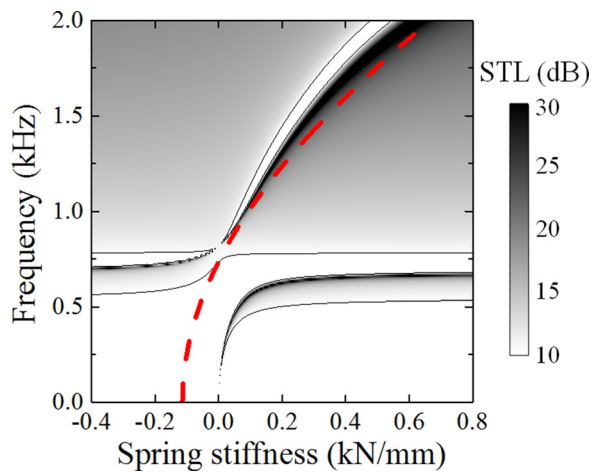

FIG. 7. The STL spectrum plotted for different stiffness coefficients of the spring, in which the dashed line refers to the frequency-dependent stiffness of the active spring.

ACKNOWLEDGMENTS

This work was supported by the National Natural Science Foundation of China (Grant Nos. 11622215, 11521062, and 11572039) and the 111 Project (B16003). The support from Air Force Office of Scientific Research under Grant No. AF 9550-15-1-0016 with Program Manager Dr. Byung-Lip (Les) Lee is also acknowledged.

[1]M. Yang and P. Sheng, Annu. Rev. Mater. Res. **47**, 83 (2017).
[2]V. M. García-Chocano, S. Cabrera, and J. Sánchez-Dehesa, Appl. Phys. Lett. **101**, 184101 (2012).

[3]N. Jiménez, V. Romero-García, V. Pagneux, and J.-P. Groby, Sci. Rep. **7**, 13595 (2017).
[4]M. Yang, S. Chen, C. Fu, and P. Sheng, Mater. Horiz. **4**, 673 (2017).
[5]Z. Liu, X. Zhang, Y. Mao, Y. Y. Zhu, Z. Yang, C. T. Chan, and P. Sheng, Science **289**, 1734 (2000).
[6]S. Yao, X. Zhou, and G. Hu, New J. Phys. **10**, 043020 (2008).
[7]S. Yao, X. Zhou, and G. Hu, New J. Phys. **12**, 103025 (2010).
[8]N. Fang, D. Xi, J. Xu, M. Ambati, W. Srituravanich, C. Sun, and X. Zhang, Nat. Mater. **5**, 452 (2006).
[9]Z. Yang, J. Mei, M. Yang, N. Chan, and P. Sheng, Phys. Rev. Lett. **101**, 204301 (2008).
[10]Z. Yang, H. M. Dai, N. H. Chan, G. C. Ma, and P. Sheng, Appl. Phys. Lett. **96**, 041906 (2010).
[11]C. J. Naify, C.-M. Chang, G. McKnight, and S. Nutt, J. Appl. Phys. **108**, 114905 (2010).
[12]Y. Chen, G. Huang, X. Zhou, G. Hu, and C.-T. Sun, J. Acoust. Soc. Am. **136**, 969 (2014).
[13]Y. Chen, G. Huang, X. Zhou, G. Hu, and C.-T. Sun, J. Acoust. Soc. Am. **136**, 2926 (2014).
[14]C. J. Naify, C.-M. Chang, G. McKnight, and S. Nutt, J. Appl. Phys. **110**, 124903 (2011).
[15]C. J. Naify, C.-M. Chang, G. McKnight, F. Scheulen, and S. Nutt, J. Appl. Phys. **109**, 104902 (2011).
[16]M. B. Assouar, M. Senesi, M. Oudich, M. Ruzzene, and Z. Hou, Appl. Phys. Lett. **101**, 173505 (2012).
[17]Y. Xiao, J. Wen, and X. Wen, J. Sound Vib. **331**, 5408 (2012).
[18]P. Li, S. Yao, X. Zhou, G. Huang, and G. Hu, J. Acoust. Soc. Am. **135**, 1844 (2014).
[19]T. Wang, M. Sheng, and Q. Qin, J. Acoust. Soc. Am. **141**, 1161 (2017).
[20]F. Langfeldt, J. Riecken, W. Gleine, and O. von Estorff, J. Sound Vib. **373**, 1 (2016).
[21]I. V. Shadrivov, A. B. Kozyrev, D. W. van der Weide, and Y. S. Kivshar, Appl. Phys. Lett. **93**, 161903 (2008).
[22]X. Chen, X. Xu, S. Ai, H. Chen, Y. Pei, and X. Zhou, Appl. Phys. Lett. **105**, 071913 (2014).
[23]S. Xiao, G. Ma, Y. Li, Z. Yang, and P. Sheng, Appl. Phys. Lett. **106**, 091904 (2015).
[24]J. Cheer, S. Daley, and C. McCormick, Smart Mater. Struct. **26**, 025032 (2017).
[25]H. Zhang, J. Wen, Y. Xiao, G. Wang, and X. Wen, J. Sound Vib. **343**, 104 (2015).
[26]H. Zhang, Y. Xiao, J. Wen, D. Yu, and X. Wen, Appl. Phys. Lett. **108**, 141902 (2016).
[27]Y. Y. Chen, G. K. Hu, and G. L. Huang, Smart Mater. Struct. **25**, 105036 (2016).
[28]N. W. Hagood and A. Vonflotow, J. Sound Vib. **146**, 243 (1991).
[29]A. Liu, X. Zhou, G. Huang, and G. Hu, J. Acoust. Soc. Am. **132**, 2800 (2012).